Korean J. Chem. Eng., 38(11), 2313-2323 (2021)
DOI: 10.1007/s11814-021-0881-6

pISSN: 0256-1115
eISSN: 1975-7220

Optimization of UV-photografting factors in preparation of polyacrylic-polyethersulfone forward osmosis membrane using response surface methodology

Ahmad Fikri Hadi Abdul Rahman*, Zulsyazwan Ahmad Khushairi*, Mazrul Nizam Abu Seman*,,†, and Mohamed Khayet***,****

*Faculty of Chemical and Process Engineering Technology, Universiti Malaysia Pahang, Lebuhraya Tun Razak, 26300 Gambang, Kuantan, Pahang, Malaysia
**Earth Resources and Sustainability (ERAS) Center, Universiti Malaysia Pahang, Lebuhraya Tun Razak, 26300 Gambang, Kuantan, Pahang, Malaysia
***Department of Structure of Matter, Thermal Physics and Electronics, Faculty of Physics, University Complutense of Madrid, Av. Complutense s/n, 28040, Madrid, Spain
****Madrid Institute for Advanced Studies of Water (IMDEA Water Institute), Calle Punto Net N° 4, 28805, Alcalá de Henares, Madrid (Spain)
(*Received 18 March 2021 • Revised 17 May 2021 • Accepted 27 June 2021*)

Abstract−Commercial nanofiltration polyethersulfone (NF2) membrane was modified via ultraviolet (UV) photografting to prepare a high-performance forward osmosis (FO) membrane. The optimized condition of grafting parameters was obtained using central composite design (CCD) and response surface methodology (RSM). UV-photografting time and acrylic acid (AA) monomer concentration were the considered variables, while the two RSM responses were water permeate flux and reverse salt diffusion flux (RSD). Quadratic models were established between the responses and the independent parameters using analysis of variance (ANOVA). The membranes were characterized with functional group, morphology and surface roughness. The obtained optimum conditions were 2.81 min grafting time and 27.85 g/L AA monomer concentration. Under these conditions, a maximum water permeate flux of 1.52±0.04 L/m^2·h was achieved with an RSD value of 10.09±0.36 g/m^2·h. The optimized membrane exhibited a higher water flux compared to the unmodified NF2 membrane without any significant change of the RSD value.

Keywords: UV-photografting, Forward Osmosis, Central Composite Design, Water Flux, Reverse Salt Diffusion

INTRODUCTION

With the rapid development in membrane technology, forward osmosis (FO) is considered a suitable emerging alternative for conventional membrane processes. This is attributed to its lower capital and operating costs, better efficiency, longer life cycle and less operating area [1]. However, the used FO membranes suffer from the known problem associated with the internal concentration polarization (ICP) phenomenon, which significantly reduces the net osmotic driving force and increases the reverse salt diffusion flux (RSD) through the membrane [2,3]. ICP occurs due to the reduction of the solute concentration of the draw solution in the porous support layer of the membrane and the interface between the active layer of the membrane and the support [2,4]. Therefore, it is of a great interest to design an FO membrane with low ICP coefficient in order to produce high permeate fluxes and low reverse salt diffusion flux. One of the strategies to improve water flux while maintaining lower reverse salt diffusion flux is by chemical modifications of FO membrane. Detailed chemical modification strategies for FO membranes can be found elsewhere [5].

Considering that both reverse osmosis (RO) and nanofiltration (NF) membranes have quite similar structure and functional properties to FO membrane, these two types of membranes are used either directly or modified for FO applications [6]. Therefore, various attempts have been made to explore the suitability of commercial RO (e.g., BW30, SW30-XLE, SW30HR, AG) and NF (e.g., NF90, NF270, SR2, HF Nano T4, HFN300) membranes in FO technology [6-13]. Besides, several efforts have been made to modify these commercial RO and NF membranes to improve their FO performance. Arena et al. [7] modified the support layer of RO membranes (BW30 and SW30-XLE) using polydopamine (PDA) and found that the water permeate flux increased up to 4-6 times with respect to the unmodified membranes. In another study [9], different RO membranes (BW30, SW30HR, AG) were treated with acids (nitric acid, sulfuric acid and phosphoric acid) and an organic solvent (ethanol) and a remarkable enhancement of the water permeate flux was observed. Jafarinejad et al. [13] investigated chemical grafting of the commercial NF membrane (NFS, Synder Filtration) using PEI (polyethylenimine) monomer at different concentrations for ammonium removal by FO process. After this chemical grafting modification, the permeate flux was increased by up to two times with respect to the unmodified NFS. Despite all the above successfully proposed modification approaches of commercial RO and NF membranes confirmed by the water permeate flux im-

†To whom correspondence should be addressed.
E-mail: mazrul@ump.edu.my

provement and the reduction of the RSD flux, the necessary required time of 1-42 h [7], 24 h [9] and 15 h [13] for such modifications is too long and not practical for industrial scale membrane production.

In our previous research [14] we suggested an alternative membrane modification route to reduce the ICP factor of FO membranes. Specifically, UV-photografting technique was conducted to reduce the ICP phenomenon by lowering the structural parameter of the membrane [14,15]. A new hydrophilic polyacrylic polymer was formed on the active layer of a supported membrane having a porous substrate layer, facilitating water transport and increasing the FO water permeate flux [14].

UV-photografting technique has been widely used due to its several advantages compared to other approaches. It does not require any pretreatment, uses less monomer for polymerization, and is a relatively simple, energy-efficient, and cost-saving technique [15,16]. For UV-photografting modification, generally four main factors affect the membrane properties and directly influence the performance of the modified membrane. The first factor is the grafting time required for a membrane to absorb the energy from UV light to form free radicals [16,17]. The second factor is the monomer concentration, which represents the necessary available functional group that is normally linked with different operating conditions, including pH, reactivity and valence [18,19]. The third factor is the UV intensity, which is related to the required energy to initiate the grafting process by opening polymer chains towards the monomer solution [20,21]. The fourth factor is the adequate monomer selection for a given application [22,23]. In general, it was observed that UV-photografting surface membrane modification resulted in an increased hydrophilicity, improved biocompatibility and functionality of membranes, and research studies were focused mainly on the two factors, grafting time and monomer concentration, because of their significantly predominant impact on membrane surface modification [24,25].

In this study, polyethersulfone (PES) membrane was selected for surface modification due to its photosensitivity. This polymer generates active sites upon UV radiation due to the excitation of phenoxyphenyl sulfone chromophores in the polymer backbone [18,26]. In addition, PES membranes exhibit good mechanical properties, high chemical and thermal stability [27,28]. In our previous work [14], hydrophilic monomer acrylic acid (AA) was selected because the carboxylic acid (-COOH) functional group could be attached to PES backbone during UV-photografting process forming polyacrylic acid polymer [29].

Response surface methodology (RSM), which involves a statistical design of experiments (DoE), a mathematical algorithm and a statistical analysis, has been applied to improve and optimize various membrane processes, even in the presence of complex interactions between factors using a minimum number of experiments [30,31]. The experimental results obtained from the designed experiment are generally compiled in mathematical models consisting of second-order polynomial functions. The developed models are then validated by statistical techniques followed by optimization [32-36]. To the best of our knowledge, no previous research studies have been reported on the optimization of UV-photografting modification of commercial NF membranes for FO application. In this study, central composite design (CCD) has been applied to model and optimize surface modification of commercial nanofiltration PES (NF2) membrane via UV-photografting for FO application.

MATERIALS AND METHODS

1. Materials

The flat sheet nanofiltration PES membrane (NF2, Amfor Inc., China) was used as substrate for UV-photografting. This membrane has a water flux of 100 L/m^2·h at 25 °C and 10.34×10^5 Pa as indicated by the manufacturer. For UV-photografting modification, the acrylic acid (AA) monomer was procured from Merck, Germany.

2. UV-photografting Polymerization

First, the membrane samples were immersed in deionized (DI) water overnight to ensure the protective layer was completely removed from the membrane surface. Subsequently, each sample was immersed in acrylic acid solution (50 ml) with a predetermined AA concentration ranging from 7.5 to 37.5 g/L and kept under a gentle stirring for 15 min. The grafting process was conducted under UV light at a predetermined grafting time. The surface modification was conducted using the UV lamp (λ=365 nm) Blak-Ray B-100 Series from UVP. The photo-reactor was a 15 cm×15 cm square stainless-steel black chamber. The membrane was fixed in a petri dish as shown in Fig. 1 and an ultraviolet (UV) lamp was placed at the top center of the chamber. The distance between the UV lamp and the membrane sample was maintained at 10 cm to provide UV irradiation energy of 15 W·m·cm^{-2}. To apply a stable intensity, the UV lamp had to be turned on 15 min before the exposing of the membrane to UV light. The modified membrane was then rinsed with DI water and stored overnight for further use.

3. Membrane Characterization

The pristine NF2 and UV-photografted membranes were characterized by means of FTIR-ATR spectrometry (Nicolet iS5, Thermo Fisher Scientific) and their morphology was analyzed by multimode atomic force microscopy (AFM) INTEGRA Prima. For each scanned sample, three different locations with about 1 μm×1 μm area were chosen arbitrarily to determine the average roughness values. The surface roughness from 512 data points was estimated as:

$$S_a = \frac{1}{N_p}\Sigma_{i=0}^{N_p}|Z_i - Z_{avg}| \quad (1)$$

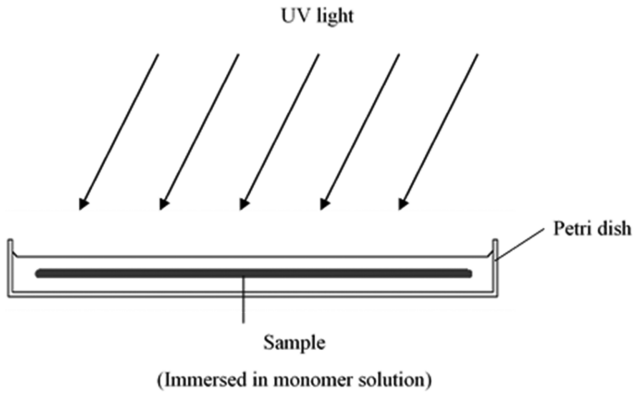

Fig. 1. UV-photografting immersion method.

Table 1. Values of actual and coded independent variables used in the experimental design

Variables	Unit	Actual and coded values				
		$-\alpha$	−1	0	+1	$+\alpha$
Grafting time	min	1	2	3	4	5
Monomer concentration	g/L	7.5	15	22.5	30	37.5

where Z_i and Z_{avg} are the current height and the average height value of the selected area, respectively.

4. Design of Experiment (DoE)

Central composite design (CCD) was considered to design the membrane modification conditions [35]. In this study, the investigated processing variables are the monomer concentration and the grafting time, while the measured response parameters are the FO water permeate flux (J_w) and the reverse salt diffusion flux (RSD). Analysis of variance (ANOVA) was used to analyze the responses based on the *p* value with confidence level of 95%. Table 1 shows the real values and coded levels of the experimental independent variables. The CCD consisted of five levels, including the center point (0), axial points ($-\alpha$=−2 & $+\alpha$=+2) and factorial points (+1 & −1).

The experimental design and optimized regression equations were developed using Design-Expert (version 7.0). The design involved 13 sets of experiments as summarized in Table 2, which consist of six center points. The experiments were conducted in the same run order as suggested by the software.

5. Forward Osmosis Performance

The used FO system, schematized in Fig. 2, consists of two tanks with a capacity of 1 L and equipped with Acrylic Sterlitech CF042 Cell having an effective area (A) of 0.0042 m^2. Both the feed (DI water) and the draw (1 M of NaCl) solutions were circulated for 1 h using a two heads peristaltic pump (model BT600-2J, Longer-Pump with two heads) at a constant flow rate of 167 ml/min. The weight changes of the feed solution were monitored with an electronic balance connected to a computer.

Table 2. Number of runs used to model the modification of the NF2 membrane by UV-photografting technique

Run	Membrane	Input variables	
		Grafting time (min)	Monomer concentration (g/L)
N		x_1	x_2
1	22.5AA-3	3	22.5
2	22.5AA-1	1	22.5
3	30AA-4	4	30.0
4	22.5AA-3	3	22.5
5	37.5AA-3	3	37.5
6	22.5AA-3	3	22.5
7	30AA-2	2	30.0
8	22.5AA-3	3	22.5
9	15AA-2	2	15.0
10	7.5AA-3	3	7.5
11	22.5AA-3	3	22.5
12	22.5AA-5	5	22.5
13	15AA-4	4	15.0

The registered weights of the feed solution were converted to volumes using the water density (ρ=1,000 kg/m^3) and finally the FO water permeate flux was determined as:

$$J_v = \frac{\Delta V}{A\Delta t} \tag{2}$$

where ΔV is the volume obtained during the predetermined FO operation time Δt=1 h and A is the effective membrane area.

The reverse salt diffusion flux (RSD) was calculated using the following equation [21]:

$$RSD = \frac{C_t V_t - C_o V_o}{A\Delta t} \tag{3}$$

where C_o and C_t are the initial and final draw solute (NaCl) concentration in g/L, respectively; and V_t and V_o represent the final

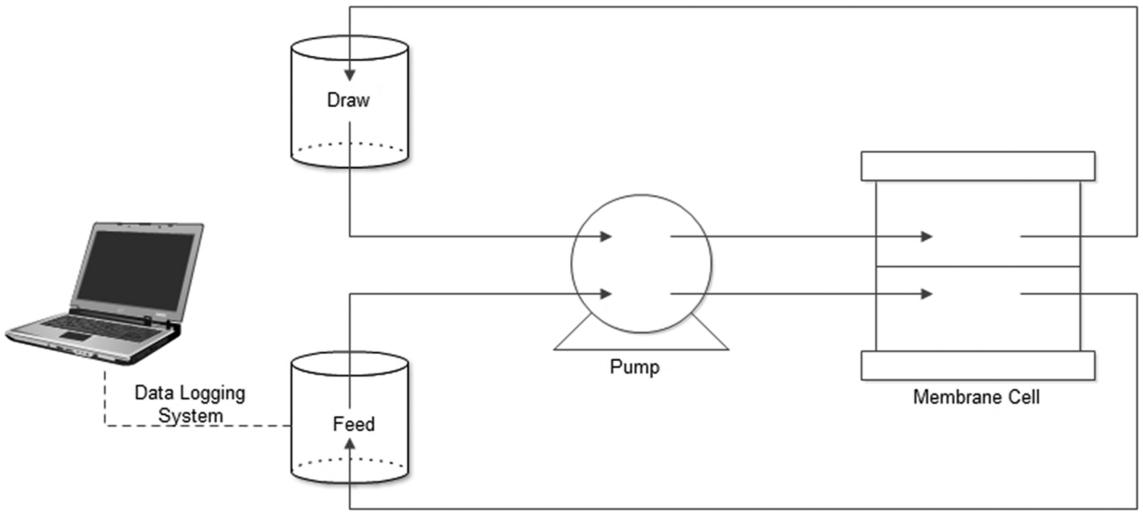

Fig. 2. FO experimental set-up.

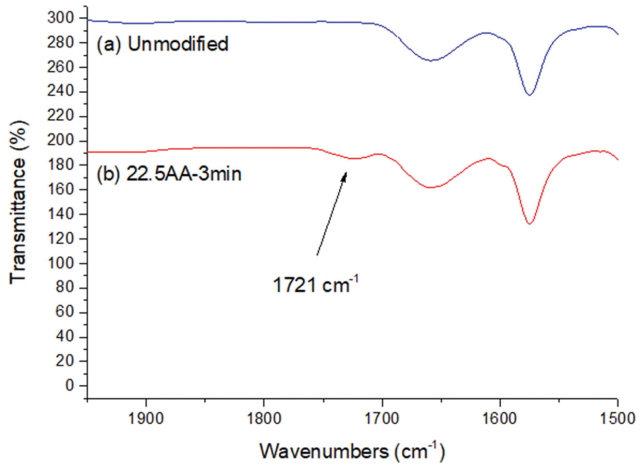

Fig. 3. FTIR-ATR of the pristine NF2 membrane and the UV-photografted membrane (22.5AA-3min).

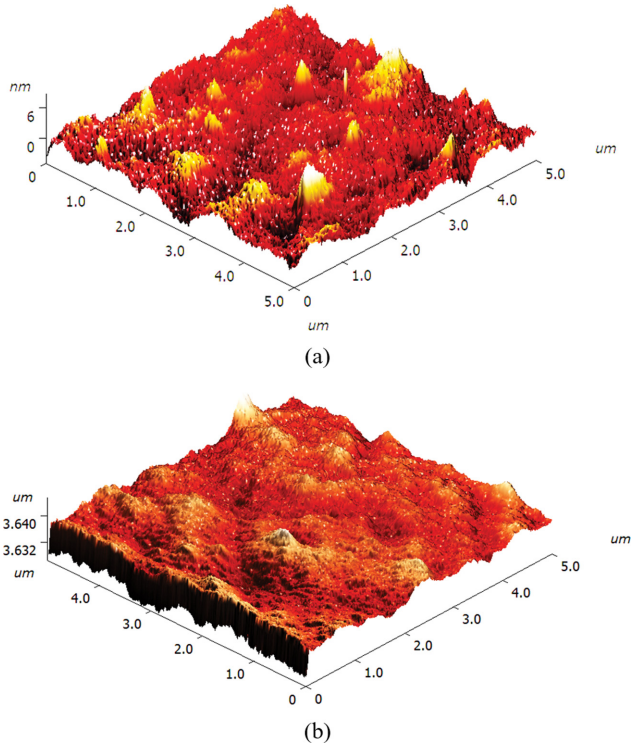

Fig. 4. AFM images of the top surface of the pristine NF2 membrane (a) and the UV-photografted membrane (22.5AA-3min) (b).

and initial volumes of the feed solution in L, respectively. Both the initial and final concentrations of the NaCl were measured by the electrical conductivity meter (Eutech, PC2700).

RESULTS AND DISCUSSION

1. Membrane Characterization

Fig. 3 shows as an example the FTIR-ATR spectra of the pristine NF2 membrane and the UV-photografted modified membrane (22.5AA-3min). The modified membrane revealed a stretching band at 1,721 cm^{-1} attributed to the carboxyl groups that were covalently bonded with the PES polymer matrix [18]. This result was also observed for other UV-photografted modified membranes reported in other studies [15,37-39].

Surface modification involves graft polymerization on the backbone of PES, where the carboxyl groups from the acrylic acid are covalently bonded [36]. During the grafting process, the phenoxyphenyl sulfone chromophores in PES chain adsorb UV-light and turn into an excited state. As a result, two radical sites are formed due to homolytic cleavage at the carbon-sulfur bond within the sulfone linkage [18]. Then, the active sites made of aryl and sulfonyl radicals react with the monomer solution (i.e., acrylic acid) to form the polyacrylic polymer with chain of the carboxyl group [40]. Note that the presence of this functional group can be associated with the enhancement of the hydrophilic character of the UV-photografted membrane and subsequent increase of water transport through the membrane active layer as reported by Pardeshi and Mungray [15] and Vatanpour et al. [38].

The top surface of both the pristine NF2 and the UV-photografted membranes was studied by atomic force microscopy (AFM). For sake of comparison all AFM images were treated following the same procedure. The obtained tridimensional topographic images are shown in Fig. 4 and the details of the surface roughness characteristics are summarized in Table 3. As can be seen, after UV-photografting, the membrane surface becomes rougher. A similar result was observed by Abuhabib et al. [41] for polyethersulfone NF membranes modified by UV-photografting using acrylic acid.

2. FO Performance

Initially, the measured water permeate flux (J_w) and the reverse salt diffusion flux (RSD) of the unmodified NF2 membrane were 0.75 $L/m^2 \cdot h$ and 9.84 $g/m^2 \cdot h$, respectively. Upon UV-photografting, all membranes exhibited significantly improved water permeate fluxes as shown in Table 4. The highest water permeate flux (1.415 $L/m^2 \cdot h$) was recorded for the membrane 22.5AA-3 (run 4), with a lower RSD value (8.9 $g/m^2 \cdot h$) than that of the unmodified NF2 membrane.

Normally, it is expected that the grafting process should occur only on the top surface of the PES membrane. However, it was observed that the grafting process also occurred inside the mem-

Table 3. Roughness values of the pristine NF2 and the UV-photografted membranes obtained from AFM analysis

No.	Membrane	Roughness (S_a, nm)	Root mean square (S_q, nm)	Maximum peak (S_z, nm)
1	NF2	1.109	1.466	9.004
2	22.5AA-3min	1.28	1.68	11.94

Table 4. J_w and RSD values of the UV-photografted membranes

Run N	Membrane	Responses	
		J_w (L/m^2·h)	RSD (g/m^2·h)
1	22.5AA-3	1.362	8.63
2	22.5AA-1	1.232	12.38
3	30AA-4	1.060	8.622
4	22.5AA-3	1.415	8.90
5	37.5AA-3	1.012	5.61
6	22.5AA-3	1.400	9.41
7	30AA-2	1.295	9.69
8	22.5AA-3	1.400	9.42
9	15AA-2	1.267	11.39
10	7.5AA-3	1.075	9.77
11	22.5AA-3	1.385	8.95
12	22.5AA-5	0.975	9.97
13	15AA-4	1.230	10.00

brane porous layer. It was reported that the monomer AA solution could penetrate into the PES membrane layer up to 20 μm and subsequently form polyacrylic polymer by means of UV-light (λ= 365 nm) [26]. As shown in Fig. 5(a), the thin top layer is approximately 323.8 nm thick, hence the light could reach the support layer of the PES membrane (Fig. 5(b)). Therefore, it may be postulated that the applied UV energy in this work was sufficient to penetrate both the thin top layer and part of the support layer affecting therefore the water permeate flux and the RSD flux.

As summarized in Table 5, the UV-photografted membranes developed in the present study exhibit higher FO water permeate flux than the commercial NF membranes (NF270, NF90 and NFS). In addition, the results reveal that all UV-photografted membranes are well formed. For instance, the NF90 membrane showed a water permeate flux of only 0.9 and 0.4 L/m^{2}h when 2 M $MgCl_2$ (π=132 bar) and 2 M $MgSO_4$ (π=57.5 bar) were used as draw solutions, respectively. Low water permeate fluxes were also observed for NF270 and NFS membranes for the same draw solutions. Interestingly, for the low 1 M NaCl concentration draw solution, which has an equivalent osmotic pressure of π=46.1 bar, the UV-photografted membrane (22.5AA-3) achieved the highest water permeate flux, 1.415 L/m^2·h. It is expected that the prepared UV-photografted membranes could achieve higher water permeate fluxes than the reported values in Table 5 if divalent ions (2 M $MgCl_2$ and 2 M $MgSO_4$) were employed to prepare the draw solution. This is because $MgCl_2$ could induce faster migration of water molecules across the FO membrane compared to the NaCl draw solution at the same concentration. It must be mentioned that osmotic pressure for $MgCl_2$ was almost double the value generated by NaCl for the same draw solution concentration [42]. When comparing the UV-photografted membranes with the chemical grafting method using PEI as monomer, the water permeate fluxes of the NF PEI-grafted membrane were lower (0.37-1.32 L/m^2·h) [13].

The reverse salt diffusion (RSD) flux of the above mentioned membranes is also summarized in Table 5. The data shows that the RSD values of the commercial NF membranes, except NFS, are lower than those of UV-photografted membranes. However, a direct comparison is not adequate since different salts were used to prepare the draw solutions. The lower RSD values obtained for NF90 and NF270 membranes occur because the divalent ion salts ($MgCl_2$ and $MgSO_4$) have larger size than the monovalent ion (NaCl) applied in this study. The smaller ionic size of NaCl compared to $MgCl_2$ and $MgSO_4$ leads to a greater salt diffusion from the permeate to the feed side of the membrane, resulting in a higher RSD value. A similar result was also observed by other authors [42-44] when comparing the FO performance of the commercial CTA membrane (HTI, Albany USA) using $MgCl_2$ and NaCl aqueous draw solutions. The commercial NFS membrane showed the highest RSD value, 13.0 g/m^2·h (i.e. 10.38 for Cl^{-1} and 2.60 for Mg^{2+}), although the same draw solution ($MgCl_2$) was used for FO testing of NF90 and NF270 membranes. This is due to the different characteristics of the NFS membrane, especially its larger pore size that cannot prevent the diffusion of $MgCl_2$ to the feed side. Note that the RSD value of Cl^- ion is higher than that of Mg^{2+} ion (e.g., NFS and NF PEI-grafted membranes in Table 5) due to different membrane selectivity towards monovalent vs. divalent ions [13]. The

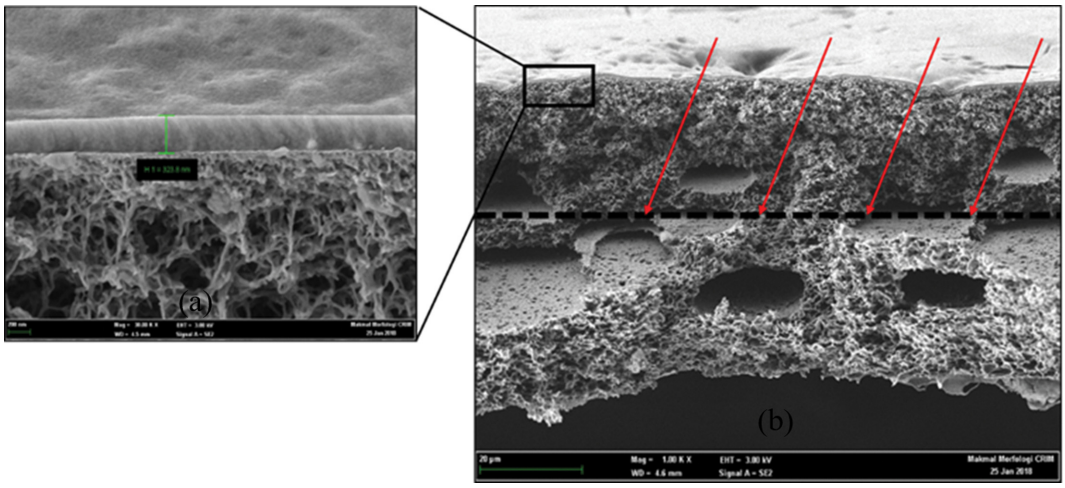

Fig. 5. SEM cross-sectional images of an UV-photografted membrane (a) thin top layer and (b) overall support layer (≈60 μm) [14].

Table 5. FO performance of different NF membranes

Membrane	Manufacturer	Material	Draw solution (Osmotic pressure)*	J_w (L/m^2·h)#	RSD (g/m^2·h)#	Ref.
Commercial NF						
NF90	Dow Film Tech	Polyamide/polysulfone support	2 M $MgCl_2$ (132 bar)	0.9	0.85	[10]
			2 M $MgSO_4$ (57.5 bar)	0.4	0.75	[10]
			35 gL^{-1} RSS (-)	1.0	0.33	[11]
NF270	Dow Film Tech	Polyamide/polysulfone support	2 M $MgSO_4$ (57.5 bar)	1.25	1.4	[10]
NFS	Synder Filtration	Polyamide/polysulfone	1 M $MgCl_2$ (66.2 bar)	0.7	10.38(Cl^{-1}), 2.60(Mg^{2+})	[13]
NF2	Amfor China	Polyethersulfone	1 M NaCl (46.1 bar)	0.75	9.84	This work
UV-grafting (using NF2 as substrate)		Polyacrylic acid/polyethersulfone	1 M NaCl (46.1 bar)			This work
22.5AA-3				1.362	8.63	
22.5AA-1				1.232	12.38	
30AA-4				1.060	8.622	
22.5AA-3				1.415	8.90	
37.5AA-3				1.012	5.61	
22.5AA-3				1.400	9.41	
30AA-2				1.295	9.69	
22.5AA-3				1.400	9.42	
15AA-2				1.267	11.39	
7.5AA-3				1.075	9.77	
22.5AA-3				1.385	8.95	
22.5AA-5				0.975	9.97	
15AA-4				1.230	10.00	
Chemical grafting (Using NFS as substrate)		Polyethylenimine (PEI)/ polyamide/polysulfone	1 M $MgCl_2$ (66.2 bar)			[13]
0.2% PEI-NFS				1.0	8.37(Cl^{-1}), 2.60(Mg^{2+})	
0.6% PEI-NFS				0.47	6.35(Cl^{-1}), 2.02(Mg^{2+})	
1.0% PEI-NFS				0.37	5.77(Cl^{-1}), 2.02(Mg^{2+})	
1.5% PEI-NFS				1.1	5.77(Cl^{-1}), 2.02(Mg^{2+})	
3.0% PEI-NFS				1.32	5.77(Cl^{-1}), 2.02(Mg^{2+})	
4.5% PEI-NFS				0.65	3.46(Cl^{-1}), 1.44(Mg^{2+})	

*Calculated using Omni Calculator (https://www.omnicalculator.com/chemistry/osmotic-pressure#coefficients-for-osmotic-pressure-formula)
#mode of operation: AL-FS (Active Layer-Feed Side) and feed solution using DI water

Table 6. Regression coefficients of J_w and RSD based on the coded variables indicated in Eq. (4)

Response	Coefficients					
	b_0	b_1	b_2	b_{11}	b_{22}	b_{12}
J_w (L/m^2·h)	1.39	−0.06	−0.02	−0.07	−0.08	−0.04
RSD (g/m^2·h)	9.25	−0.61	−0.95	0.54	−0.33	0.08

Table 7. Regression coefficients of J_w and RSD based on the actual variables indicated in Eq. (5)

Response	Coefficients					
	γ_0	γ_1	γ_2	γ_{11}	γ_{22}	γ_{12}
J_w (L/m^2·h)	−0.23	0.51	0.08	−0.07	-1.55×10^{-3}	-6.5×10^{-3}
RSD (g/m^2·h)	16.52	−4.08	0.1	0.53	-5.88×10^{-3}	0.01

RSD fluxes of the NF PEI-grafted membranes are in the range 4.9-11 g/m^2·h when using 1 M $MgCl_2$ aqueous draw solution and those of the UV-photografted membranes are slightly higher, 5.61-12.38 g/m^2·h but using 1 M NaCl aqueous draw solution. Although both types of grafted membranes show almost similar RSD values, the UV-photografted membrane is better because of its higher ability to prevent reverse salt diffusion, smaller size solute (NaCl) in this case. Therefore, optimization of the UV-photografting parameters is required and it is discussed in detail in the next section.

3. RSM Models

Based on the developed experimental design, second-order polynomial models with interactions were developed for both responses, J_w and RSD, as indicated in Eqs. (4) and (5) for coded and actual factors, respectively.

$$Y=b_0+b_1x_1+b_2x_2+b_{11}x_1^2+b_{22}x_2^2+b_{12}x_1x_2 \quad (4)$$

$$Y=\gamma_0+\gamma_1C+\gamma_2t+\gamma_{11}C^2+\gamma_{22}t^2+\gamma_{12}Ct \quad (5)$$

where x_1 and x_2 are the coded independent variables, Y is the predicted response, t is the grafting time, C is the monomer concentration, b_0, b_2, b_{11}, b_{22} and b_{12} in Eq. (4) and γ_0, γ_2, γ_{11}, γ_{22} and γ_{12} in Eq. (5) are the regression coefficients.

The regression coefficients were computed in order to minimize the sum of squares of the residuals. The obtained values of the regression coefficients calculated based on the coded factors are summarized in Table 6, whereas those based on the actual variables are presented in Table 7.

The normal plot of residuals together with the residuals *versus* predicted values of both J_w and RSD are shown in Figs. 6 and 7, respectively. For both responses, the normal plot of residuals are straight lines with reasonably high correlation coefficients (R^2 value of 0.9875 and 0.9348 for J_w and RSD, respectively), suggesting that the errors are scattered normally, which supports the suitability of the least-square fit. In addition, as can be seen in Figs. 6(b) and 7(b), the results are scattered equally on both *x*-axes, proving no obvious pattern and unusual behavior to discard the models.

Analysis of variance (ANOVA) was applied to validate statistically the developed RSM models and identify the main factors that are statistically significant. The obtained ANOVA results are summarized in Table 8 for J_w. The obtained *F* value (110.86) implies that the model gives a good prediction of the experimental data.

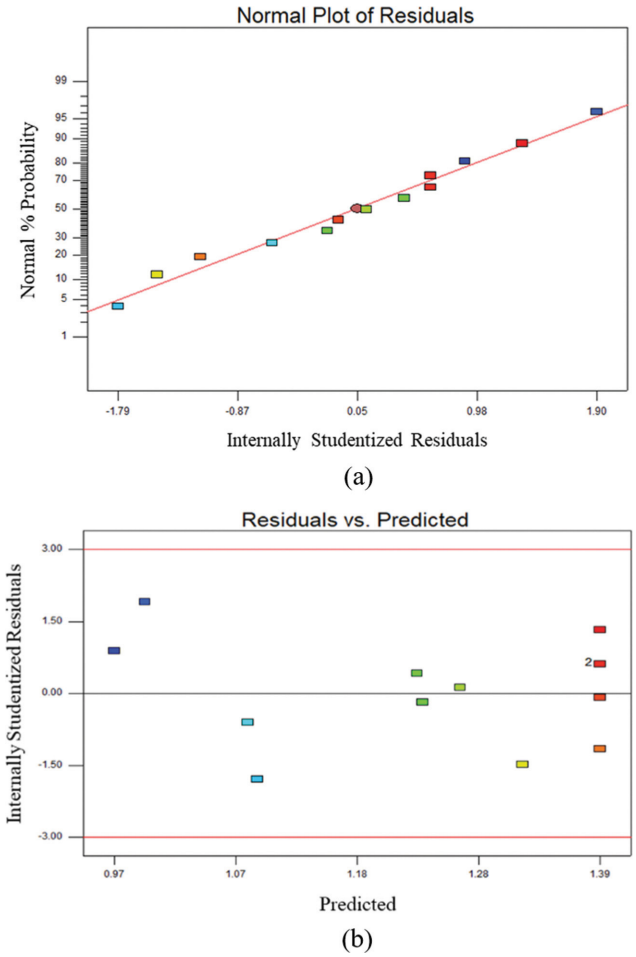

Fig. 6. Normal plot of residuals (a) and plot of residuals *vs.* predicted values, (b) for the water permeate flux (J_w).

Moreover, the *p* value of 0.2757 indicates that the lack of fit is insignificant. In addition, the obtained R^2 value (0.9875) is higher than the adjusted statistics R^2 value (0.9786), indicating that only significant terms have been included in the empirical model. In general, the values from ANOVA indicate a good agreement between the predicted and experimental J_w values of the UV-photografted membranes. Therefore, the RSM model can be applied

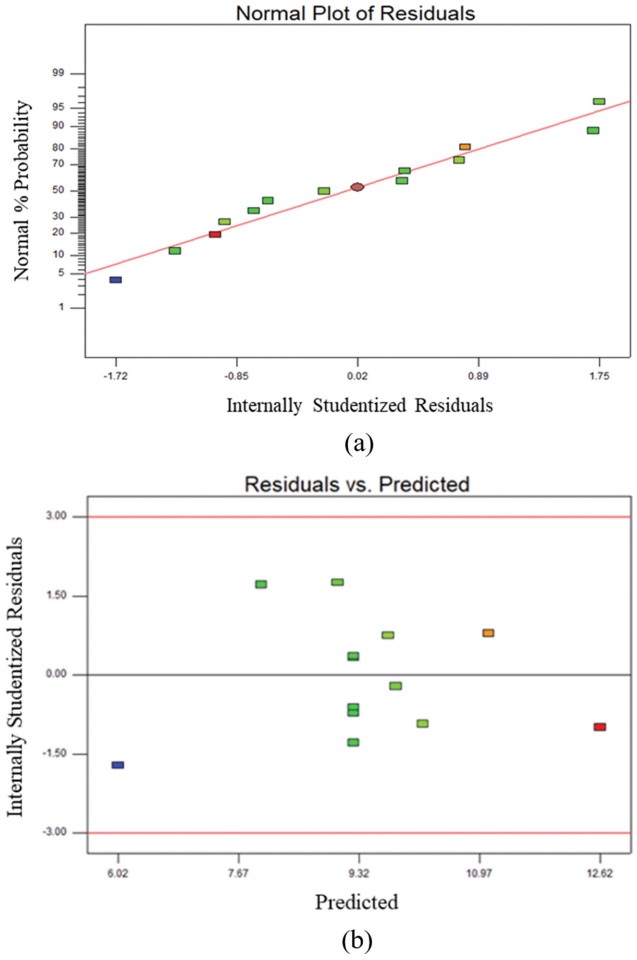

Fig. 7. Normal plot of residuals (a) and plot of residuals vs. predicted values, (b) for the reverse salt diffusion flux (RSD).

to predict the optimum grafting parameters for a maximum water permeate flux.

The same procedure was applied to RSD and the obtained ANOVA results are shown in Table 9. The computed *F* value (20.07) indicates a good prediction of the experimental RSD data, while the lack of fit of this RSM model is insignificant as the registered *p* value is 0.1027. Only significant terms have been included in the empirical model as the obtained R^2 value (0.9348) was found to be higher than the adjusted statistics R^2 value (0.8882). However, the predicted R^2 value is low (0.6189) due to the interaction of monomer concentration and grafting time (AB=0.026). In general, it can be concluded that the predicted and experimental RSD values of the UV-photografted membranes are also in good agreement.

The effects of the monomer concentration (B) and UV-grafting time (t) on the water permeate flux (J_w) are plotted in Fig. 8. An optimum condition can be identified. A gradual decrease of J_w can be seen with the increase of UV-grafting time. This can be explained by the development of the grafted layer on the PES membrane surface. According to Mansourpah and Habili [25], the longer the UV radiation period, the better the polymerization degree, such that a denser thin layer can be formed. With the increase of the AA monomer concentration, an enhancement of J_w up to a maximum was detected followed by a slight decline. A similar trend was also reported by Pardeshi and Mungray [15] for UV-photografted modified FO membranes using methacrylic acid (MAA) as monomer. The grafting time of 3 min and a monomer concentration of 22.5 g/L resulted in a high J_w. As stated earlier, this was attributed to the increase of the hydrophilic character of the membrane surface due to the formation of carboxyl functional groups that significantly improved the membrane water permeability [15, 19,38]. It must be pointed out that the enhancement of J_w of PES by UV-irradiation was also attributed to pores enlargement [45].

The response surface plots in Fig. 9 reveal the influence of the grafting time (t) and monomer concentration (B) on RSD. At the lowest grafting time (2 min) and monomer concentration (15 g/L), the value of RSD was high (10.55 g/m^2·h). However, RSD decreased slightly as the grafting time and monomer concentration was increased (8.38 g/m^2·h). This can be attributed to the formation of a denser polyacrylic layer at a higher AA concentration hindering the passage of draw solute ions. A similar pattern of RSD reduc-

Table 8. ANOVA analysis for the developed RSM model of J_w

Source	Sum of squares	DF	Mean square	*F* value	Prob>*F*	
Model	0.30	5	0.06	110.86	<0.0001	Significant
A - Grafting Time	0.052	1	0.052	95.64	<0.0001	
B - Monomer Concentration	5.963×10^{-3}	1	5.963×10^{-3}	11.03	0.0127	
AB	9.752×10^{-3}	1	9.752×10^{-3}	18.05	0.0038	
A^2	0.12	1	0.12	223.08	<0.0001	
B^2	0.18	1	0.18	324.89	<0.001	
Residual	3.783×10^{-3}	7	5.404×10^{-4}			
Lack of Fit	2.208×10^{-3}	3	7.359×10^{-4}	1.87	0.2757	Not significant
R-squared	0.9875					
Adjusted *R*-squared	0.9786					
Predicted R-squared	0.9306					
Adequate Precision	26.682					
Std. Deviation	0.023					
Mean	1.24					

Table 9. ANOVA analysis for the developed RSM model of RSD

Source	Sum of squares	DF	Mean square	*F* value	Prob>*F*	
Model	27.8	5	5.56	20.07	0.0005	Significant
A - Grafting Time	4.41	1	4.41	15.93	0.0052	
B - Monomer Concentration	10.83	1	10.83	39.08	0.0004	
AB	0.026	1	0.026	0.094	0.7686	
A^2	6.68	1	6.68	24.11	0.0017	
B^2	2.52	1	2.52	9.08	0.0196	
Residual	1.94	7	0.28			
Lack of Fit	1.46	3	0.49	4.11	0.1027	Not significant
R-squared	0.9348					
Adjusted *R*-squared	0.8882					
Predicted R-squared	0.6189					
Adequate Precision	18.451					
Std. Deviation	0.53					
Mean	9.44					

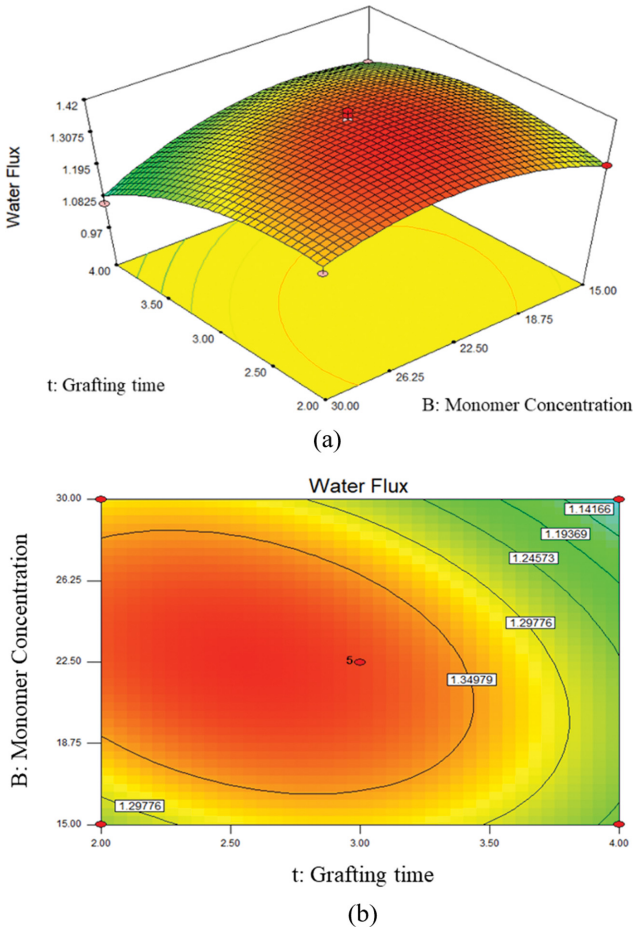

Fig. 8. Response surface plot (a) and contour plot (b) of the predicted water permeate flux (J_w) as a function of the monomer concentration (B) and grafting time (t).

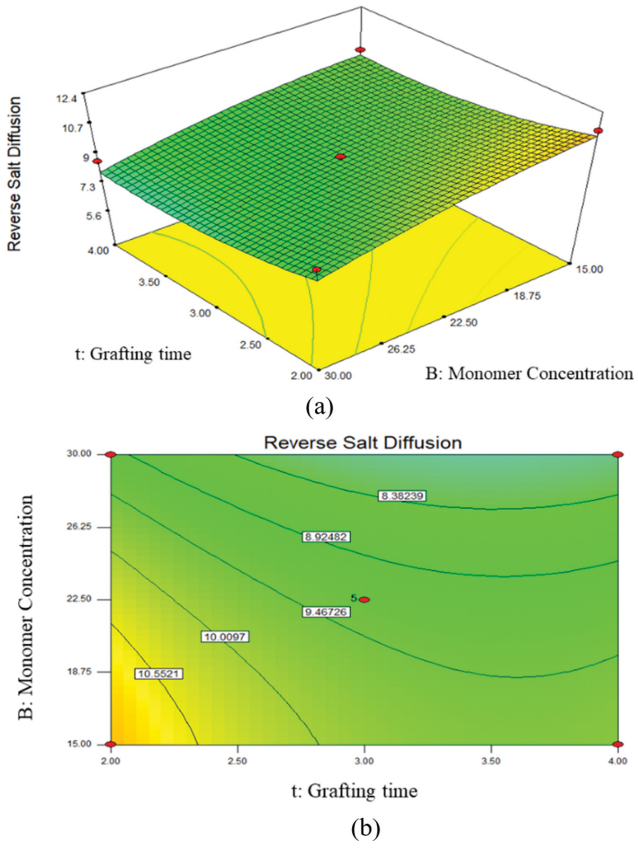

Fig. 9. Response surface plot (a) and contour plot (b) of the reverse salt diffusion flux (RSD) as a function of the monomer concentration (B) and grafting time (t).

tion was also observed for UV-photografted NF membrane with MAA [15]. Fig. 9(b) suggests that there was no interaction between t and C and the increase of both t and C had no significant effect on the RSD (<20.6%). As stated earlier, some of the modified membranes might experience pore enlargement after UV-photografting. This could result in more transport of salt from the draw solution to the feed side, increasing the RSD as a consequence.

4. Data Validation

The developed RSM models from the experimental data are

Table 10. Validation of the obtained optimum UV-photografting modification condition and the predicted and experimental responses

No.	Grafting time (min)	Monomer concentration (g/L)	Predicted J_w (L/m^2·h)	Experimental J_w (L/m^2·h)	Predicted RSD (g/m^2·h)	Experimental RSD (g/m^2·h)
1	2.81	27.85	1.4	1.55	9.41	10.21
2	2.81	27.85	1.4	1.54	9.41	9.77
3	2.81	27.85	1.4	1.48	9.41	10.28
			Average	1.52±0.04	Average	10.09±0.36
			Error percentage	7.9%	Error percentage	6.7%

suitable to predict the FO performance, water permeate flux and reverse salt diffusion flux, for any ratio of grafting time and monomer concentration inside the experimental valid region. The criteria for an optimum condition were to maximize the water permeate flux and minimize the reverse salt diffusion. The determined optimum UV-grafting condition by the Design Expert Software is summarized in Table 10 together with the experimental confirmation runs.

The determined optimum condition to modify the NF2 PES membrane and prepare an adequate FO membrane was a grafting time of 2.81 min and 27.85 g/L of acrylic acid concentration. The obtained FO membrane exhibited a maximum water permeate flux (1.52±0.04 L/m^2·h) compared to the other modified membranes with a reasonably low RSD (10.09±0.36 g/m^2·h). The agreement between the experimental and the predicted optimum values of J_w and RSD was found to be reasonably good (i.e., less than 8% deviation). The optimized FO membrane exhibited higher water permeate flux without compromising the RSD flux, and even better than the commercial NF-like FO membranes and other grafted NF membranes applied in FO technology as can be seen in Table 5.

CONCLUSIONS

The commercial nanofiltration polyethersulfone (NF2) membrane was successfully modified by UV-photografting for forward osmosis (FO) application. The modified membranes exhibit a polyacrylic layer on the porous layer, which facilitates the transport of water molecules across the membrane. Besides the increase of the hydrophilic character of the membrane, the polyacrylic layer increases the surface roughness, which leads to an increase of the membrane active area. The modified membranes exhibit better FO performance than the NF2 membrane.

The developed predictive RSM models of the FO permeate water flux and the reverse salt diffusion (RSD) flux as a function of the grafting time and monomer acrylic acid concentration were validated by analysis of variance. A gradual decrease of the water permeate flux was observed with the increase of UV-grafting time, whereas a maximum permeate flux was detected with the increase of the monomer concentration. In contrast, the RSD decreased slightly as the grafting time and the monomer concentration were increased, and no clear interaction between these two parameters was identified.

The RSM models were finally applied to predict the optimum UV-photografting parameters to prepare an FO membrane with a maximum water permeate flux and a minimum RSD. Among the two responses, the dominant response was the water permeate flux. The optimum UV-photografting conditions were an acrylic acid concentration of 27.86 g/L and a grafting time of 2.81 min being the obtained permeate water flux 1.52 L/m^2·h and the RSD 10.09 g/m^2·h.

ACKNOWLEDGEMENTS

The authors gratefully acknowledge the financial support of Universiti Malaysia Pahang under the Postgraduate Research Grant Scheme (PGRS180389), the Fundamental Research Grant Scheme (FRGS/1/2016/TK02/UMP/02/8; RDU160127), the Ministry of Higher Education, Malaysia for the PhD scholarship of Ahmad Fikri Hadi Abdul Rahman, and the support of the Spanish Ministry of Economy and Competitiveness through its project CTM2015-65348-C2-2-R and the Spanish Ministry of Science, Innovation and Universities through its project RTI2018-096042-B-C22.

NOMENCLATURE AND SYMBOLS

AA : Acrylic Acid
AFM : Atomic Force Microscopy
ANOVA : Analysis of variance
CTA : Cellulose Tri-Acetate
CCD : Central Composite Design
DI : Deionized
FO : Forward Osmosis
FS : Feed side
ICP : Internal Concentration Polarization
MAA : Methacrylic Acid
NF : Nanofiltration
PES : Polyethersulfone
PEI : Polyethylenimine
RSM : Response Surface Modelling
RSS : Red Sea Salt
UV : Ultraviolet
AL-FS : Active Layer-Feed Side
A : Membrane surface area [m^2]
b : Regression coefficient for coded factors
C : Monomer concentration [g/L]
J_w : Water permeate flux [(L/m^2·h]
Y : Predicted Response
S_a : Surface Roughness [nm]
S_q : Root mean square [nm]
S_z : Maximum peak [nm]

t : Grafting time [min]
V : Volume [L]
Z_{avg} : Average value of the height [nm]
Z_i : Current height [nm]
α : Axial point
g : Regression coefficient for actual factors

REFERENCES

1. L. Chekli, S. Phuntsho, J. E. Kim, J. Kim, J. Y. Choi, J.-S. Choi, S. Kim, J. H. Kim, S. Hong, J. Sohn and H. K. Shon, *J. Membr. Sci.*, **497**, 430 (2016).
2. W. Wang, Y. Guo, M. Liu, X. Song and J. Duan, *Korean J. Chem. Eng.*, **37**, 1573 (2020).
3. C. Bae, K. Park, H. Heo and D. R. Yang, *Korean J. Chem. Eng.*, **34**, 844 (2017).
4. Z. Zhou, J. Y. Lee and T.-S., Chung, *Chem. Eng. J.*, **249**, 236 (2014).
5. W. Xu, Q. Chen and Q. Ge, *Desalination*, **419**, 101 (2017).
6. S. Dutta, P. Dave and K. Nath, *J. Wat. Proc. Eng.*, **33**, 101092 (2020).
7. J. T. Arena, S. S. Manickam, K. K. Reimund, B. D. Freeman and J. R. McCutcheon, *Desalination*, **343**, 8 (2014).
8. J. Wei, C. Qiu, C. Y. Tang, R. Wang and A. G. Fane. *J. Membr. Sci.*, **372**(1-2), 292 (2011).
9. X. Wang, E. Duitsman, N. Rajagopalan and V. V. Namboodiri, *Desalination*, **319**, 66 (2013).
10. W. N. A. S. Abdullah, W. J. Lau, F. Aziz, D. Emadzadeh and A. F. Ismail, *Chem. Eng. Technol.*, **41**, 303 (2018).
11. G. Blandin, D. T. Myat, A. R. D. Verliefde and P. Le-Clech, *J. Membr. Sci.*, **533**, 250 (2017).
12. S. O. Alaswad, S. A. E. Alpay and A. O. Sharif, *J. Chem. Eng. Process Technol.*, **09**, 1 (2018).
13. S. Jafarinejad, H. Park, H. Mayton, S. L. Walker and S. C. Jiang, *Environ. Sci.: Water Res. Technol.*, **5**, 246 (2019).
14. A. F. H. Abdul Rahman and M. N. Abu Seman, *J. Env. Chem. Eng.*, **6**, 4368 (2018).
15. M. Pardeshi and A. A. Mungray. *Sci. Rep.*, **9**, 1937 (2019).
16. J. Zhou, W. Li, J.-S. Gu, H.-Y. Yu, Z.-Q. Tang and X.-W. Wei, *Sep. Purif. Technol.*, **71**, 233 (2010).
17. J. Garcia-Ivars, M.-I. Iborra-Clar, M.-I. Alcaina-Miranda, J.-A. Mendoza-Roca and L. Pastor-Alcañiz, *Chem. Eng. J.*, **283**, 231 (2016).
18. M. N. Abu Seman, M. Khayet, Z. I. Bin Ali and N. Hilal, *J. Membr. Sci.*, **355**(1-2), 133 (2010).
19. M. N Abu Seman, M. Khayet and N. Hilal, *Desalination*, **287**, 19 (2012).
20. P. D. Peeva, T. Pieper and M. Ulbricht, *J. Membr. Sci.*, **362**(1-2), 560 (2010).
21. J. Pieracci, J. V. Crivello and G. Belfort, *Chem. Mater.*, **14**(1), 256 (2002).
22. A. Rahimpour, *Desalination*, **265**(1-3), 93 (2011).
23. M. Taniguchi and G. Belfort, *J. Membr. Sci.*, **231**(1-2), 147 (2004).
24. Y. T. Chung, L. Y. Ng and A. W. Mohammad, *J. Ind. Eng. Chem.*, **20**(4), 1549 (2014).
25. Y. Mansourpanah and E. Momeni Habili, *J. Membr. Sci.*, **430**, 158 (2013).
26. H. Yamagishi, J. V. Crivello and G. Belfort, *J. Membr. Sci.*, **105**(3), 237 (1995).
27. L. Y. Ng, A. L. Ahmad and A. W. Mohammad, *Arabian J. Chem.*, **10**, S1821 (2017).
28. C. Zhao, J. Xue, F. Ran and S. Sun, *Prog. Mat. Sci.*, **58**(1), 76 (2013).
29. M. Ulbricht, *Polymer*, **47**(7), 2217 (2006).
30. M. Khayet, C. Cojocaru and G. Zakrzewska-Trznadel, *J. Membr. Sci.*, **321**(2), 272 (2008).
31. M. Khayet, J. Sanmartino, M. Essalhi, M. García-Payo and N. Hilal, *Solar Energy*, **137**, 290 (2016).
32. A. Solouk, M. Solati-Hashjin, S. Najarian, H. Mirzadeh and A. M. Seifalian, *Iran Polym. J.*, **20**, 91 (2011).
33. I. Xiarchos, A. Jaworska and G. Zakrzewska-Trznadel, *J. Membr. Sci.*, **321**(2), 222 (2008).
34. D. Podstawczyk, A. Witek-Krowiak, A. Dawiec and A. Bhatnagar, *Eco. Eng.*, **83**, 364 (2015).
35. F. Xiangli, W. Wei, Y. Chen, W. Jin and N. Xu, *J. Membr. Sci.*, **311**(1), 23 (2008).
36. B. Deng, J. Li, Z. Hou, S. Yao, L. Shi, G. Liang and K. Sheng, *Rad. Phy. Chem.*, **77**(7), 898 (2008).
37. O. N. Tretinnikov, V. V. Pilipenko and S. P. Firsov, *Polym. Sci., Ser. B*, **53**(3-4), 171 (2011).
38. V. Vatanpour, M. Esmaeili, M. Safarpour, A. Ghadimi and J. Adabi, *React. Funct. Polym.*, **134**, 74 (2019).
39. Z. W. Heng, W. C. Chong, Y. L. Pang and C. H. Koo, *Mater. Today Proceedings*, **46**(5), 1901 (2021).
40. B. Van der Bruggen, *J. Appl. Pol. Sci.*, **114**(1), 630 (2009).
41. A. A. Abuhabib, A. W. Mohammad, N. Hilal, R. A. Rahman and A. H. Shafie, *Desalination*, **295**, 16 (2012).
42. J. Y. Law and A. W. Mohammad, *Jurnal Teknologi (Sciences and Engineering)*, **79**(5-3), 47 (2017).
43. J. Y. Law and A. W. Mohammad, *J. Ind. Eng. Chem.*, **51**, 264 (2017).
44. J. Y. Li, Z. Y. Ni, Z. Y. Zhou, Y. X. Hu, X. H. Xu and L. H. Cheng, *J. Membr. Sci.*, **552**, 213 (2018).
45. L. Puro, M. Mänttäri, A. Pihlajamäki and M. Nyström, *Chem. Eng. Res. Des.*, **84**(2), 87 (2006).